



Synthesized 7T MPRAGE From 3T MPRAGE Using Generative Adversarial Network and Validation in Clinical Brain Imaging: A Feasibility Study

Caohui Duan, PhD,¹

Xiangbing Bian, MS,¹ Kun Cheng, BS,¹ Jinhao Lyu, MS,¹ Yongqin Xiong, MD,¹ Sa Xiao, PhD,²

Xueyang Wang, MS,¹ Qi Duan, BS,¹ Chenxi Li, BS,¹ Jiayu Huang, BS,¹ Jianxing Hu, BS,¹

Z. Jane Wang, PhD,³ Xin Zhou, PhD,²  and Xin Lou, MD^{1*} 

Background: Ultra-high field 7T MRI can provide excellent tissue contrast and anatomical details, but is often cost prohibitive, and is not widely accessible in clinical practice.

Purpose: To generate synthetic 7T images from widely acquired 3T images with deep learning and to evaluate the feasibility of this approach for brain imaging.

Study Type: Prospective.

Population: 33 healthy volunteers and 89 patients with brain diseases, divided into training, and evaluation datasets in the ratio 4:1.

Sequence and Field Strength: T1-weighted nonenhanced or contrast-enhanced magnetization-prepared rapid acquisition gradient-echo sequence at both 3T and 7T.

Assessment: A generative adversarial network (SynGAN) was developed to produce synthetic 7T images from 3T images as input. SynGAN training and evaluation were performed separately for nonenhanced and contrast-enhanced paired acquisitions. Qualitative image quality of acquired 3T and 7T images and of synthesized 7T images was evaluated by three radiologists in terms of overall image quality, artifacts, sharpness, contrast, and visualization of vessel using 5-point Likert scales.

Statistical Tests: Wilcoxon signed rank tests to compare synthetic 7T images with acquired 7T and 3T images and intraclass correlation coefficients to evaluate interobserver variability. $P < 0.05$ was considered significant.

Results: Of the 122 paired 3T and 7T MRI scans, 66 were acquired without contrast agent and 56 with contrast agent. The average time to generate synthetic images was ~11.4 msec per slice (2.95 sec per participant). The synthetic 7T images achieved significantly improved tissue contrast and sharpness in comparison to 3T images in both nonenhanced and contrast-enhanced subgroups. Meanwhile, there was no significant difference between acquired 7T and synthetic 7T images in terms of all the evaluation criteria for both nonenhanced and contrast-enhanced subgroups ($P \geq 0.180$).

Data Conclusion: The deep learning model has potential to generate synthetic 7T images with similar image quality to acquired 7T images.

Level of Evidence: 2

Technical Efficacy: Stage 1

J. MAGN. RESON. IMAGING 2023.

View this article online at [wileyonlinelibrary.com](https://onlinelibrary.wiley.com/doi/10.1002/jmri.28944). DOI: 10.1002/jmri.28944

Received Nov 27, 2022, Accepted for publication Jul 26, 2023.

*Address reprint requests to: X.L., Department of Radiology, Chinese PLA General Hospital, 28 Fuxing Road, Beijing 100853, China.

E-mail: louxin@301hospital.com.cn

The first two authors contributed equally to this work.

Contract grant sponsor: National Natural Science Foundation of China; Contract grant numbers: 81825012, 82151309, and 82202133.

From the ¹Department of Radiology, Chinese PLA General Hospital, Beijing, China; ²Key Laboratory of Magnetic Resonance in Biological Systems, State Key Laboratory of Magnetic Resonance and Atomic and Molecular Physics, National Center for Magnetic Resonance in Wuhan, Wuhan Institute of Physics and Mathematics, Innovation Academy for Precision Measurement Science and Technology, Chinese Academy of Sciences–Wuhan National Laboratory for Optoelectronics, Wuhan, China; and ³Department of Electrical and Computer Engineering, The University of British Columbia, Vancouver, British Columbia, Canada

Additional supporting information may be found in the online version of this article

Ultra-high field 7T MRI is an emerging technique, which provides images with higher resolution and signal-to-noise ratio in comparison with routine 3T and 1.5T MRI.^{1,2} 7T MRI has the potential to improve the diagnosis and monitoring of diseases such as multiple sclerosis, cerebrovascular disease, brain tumors, and aging-related brain changes.³ In addition, 7T MRI has been shown to allow better delineation of brain tissues and small anatomical substructures, such as hippocampus.⁴⁻⁶ However, 7T MRI scanners are much more expensive and infrequently available in the clinic. Currently, there are fewer than 100 7T MRI scanners compared with more than 20,000 3T MRI scanners in the world.⁵ Therefore, synthesizing 7T MR images from widely acquired 3T images may be desirable for both clinical and research applications.

Recent studies have shown that 7T images can be synthesized from 3T images using learning-based methods, such as linear regression⁶ and random forest.⁴ However, the effectiveness of these methods is typically limited by the quality of hand-crafted features.⁵ In recent years, deep learning, particularly the generative adversarial network, has been successfully used in various medical image synthesis problems.^{7,8} Nie et al proposed a deep convolutional adversarial network incorporating gradient difference loss to learn the nonlinear 3T-to-7T mapping.⁹ Qu et al introduced a deep learning network (i.e., WATNet) that leverages the wavelet domain as a prior to synthesizing 7T images with better tissue contrast and greater detail.⁵

Learning 3T-to-7T mappings generally requires large amounts of paired and well pixel-wise aligned 3T and 7T data.¹⁰ However, it is difficult to acquire abundant paired 3T and 7T data because 7T MRI scanners are not widely accessible.¹¹ Previous studies have been based on paired 3T and 7T MR scans from 15 healthy volunteers, and have used semi-supervised adversarial learning¹¹ or data augmentation¹² to learn reliable mappings from 3T scans to 7T scans. However, the feasibility of using the generated synthetic 7T images for clinical brain imaging was not evaluated.

T1-weighted magnetization-prepared rapid acquisition gradient-echo (MPRAGE) benefits substantially from the use of ultra-high field 7T MRI and provides excellent contrast between gray and white matter.¹³ Moreover, contrast-enhanced 7T MPRAGE allows better visualization of brain tumor details and higher diagnostic confidence compared with 3T MPRAGE.¹⁴

As a proof-of-concept study, the purpose of this study was to develop a generative adversarial network (SynGAN) model to synthesize high-quality 7T MPRAGE images from nonenhanced and contrast-enhanced 3T MPRAGE images, and to investigate the image quality of the synthetic 7T images in clinical brain imaging.

Materials and Methods

Study Participants

This prospective study was approved by the Institutional Review Board and was registered on [ClinicalTrials.gov](https://clinicaltrials.gov) (NCT05287750 and NCT05200377). Informed written consent was obtained from all participants. The study complied with both the Declaration of Helsinki and the Health Insurance Portability and Accountability Act.

Participants undergoing a clinical brain MRI examination or healthy volunteers were consecutively recruited at our local hospital from January 2022 to May 2022. Inclusion criteria consisted of an agreement to participate, age of 18 years or older, the ability to remain in the supine position and still for both the 3T and 7T MRI examinations. Exclusion criteria were general contraindications for MRI. Both the 3T and 7T MPRAGE images were acquired as additional scans at the radiology department of our local hospital. Contrast-enhanced 3T and 7T MRI were only acquired in part of patients. Clinical characteristics of the study participants are summarized in Table 1. The paired 3T and 7T data were acquired from 122 participants (55 men, 67 women; mean age, 42 years \pm 15), including healthy subjects and patients with tumor, cerebrovascular disease, multiple sclerosis, and other conditions. Among the 122 paired data sets, 66 were nonenhanced T1-weighted images, and 56 were contrast-enhanced T1-weighted images.

TABLE 1. Clinical Characteristics of the Study Participants

Characteristics	Nonenhanced image	Contrast-enhanced image	Total
No. of subjects	66	56	122
Age (y) ^a	36 \pm 14	49 \pm 12	42 \pm 15
Sex			
Female	41	26	67
Male	25	30	55
Clinical indication			
Brain tumor	10	45	55
Healthy	33	0	33
Cerebrovascular disease	14	7	21
Multiple sclerosis	8	2	10
Encephalitis	1	1	2
Neuromyelitis optica	0	1	1

^aData are means \pm SDs; The clinical indications of patients were confirmed from the corresponding diagnostic reports.

MRI Protocols

MRI examinations were performed on a 7T scanner (MAGNETOM Terra; Siemens Healthineers, Erlangen, Germany) using a 32-channel head coil (Nova Medical; Wilmington, MA) and a 3T scanner (MAGNETOM Skyra; Siemens Healthineers, Erlangen, Germany) using a 20-channel head coil. For both 3T and 7T MRI, T1-weighted images were acquired using a 3D MPRAGE sequence. The details of acquisition parameters are described in Table 2. Contrast-enhanced T1-weighted images were first acquired at 3T after intravenous administration of Gadolinium contrast agent (0.1 mmol/kg Gadolinium-DTPA; Beijing BeiLu Pharmaceutical Co., Ltd, Beijing, China) with high pressure injector. The time intervals between the contrast agent injection and the acquisition of 3T image and 7T image were 6 minutes 27 sec \pm 1 minutes 22 sec and 26 minutes 9 sec \pm 4 minutes 49 sec, respectively.

Data Preprocessing

The 7T images were processed with N4 bias field correction,¹⁵ and a brain mask of the 7T images was obtained by using ROBEX.¹⁶ Then, the 3T images were coregistered to the corresponding 7T images using FLIRT in FSL package with 12-parameter affine registration.¹⁷ After registration, the brain mask was applied to the 3T and 7T images for skull removal, and the intensity values of the two images were normalized to [0, 1]. The data set were randomly split into training and test datasets (80% training and 20% test). Among the nonenhanced dataset, 53 were randomly selected for training and 13 were used for testing. Among the contrast-enhanced dataset, 46 were randomly selected for training and 10 were used for testing. All of the following image evaluation and illustration was performed on the test data of 23 participants. The volume data of each participant was split into axial slices, with each slice serving as a separate

training example. There was no data overlap between the training dataset and test dataset.

Network Architecture

To synthesize 7T images with good texture details and perceptual quality, a deep learning model (SynGAN) based on a generative adversarial network was proposed.¹⁸ As shown in Fig. 1, SynGAN consists of a generator and a discriminator. The generator is used to synthesize 7T images from the corresponding 3T images, and the discriminator tries to distinguish the synthetic 7T images from the real ones. We adopted U-Net as the generator, because the U-Net has advantages of multilevel decomposition, multichannel filtering and multiscale skip connections.¹⁹ The advantages of the U-Net lead to robust and superior reconstructed images compared with other architectures.^{18,19} The detailed architecture of U-Net is provided in our previous study.²⁰ The discriminator takes the 3T image with the real 7T image or with the synthesized 7T image as an input pair, and outputs a decision variable for binary classification (see details in Fig. S1 in the Supplemental Material). The details of the network architecture are described in Methods in the Supplemental Material.

Training and Implementation Details

SynGAN was implemented using the PyTorch package (version 1.09; <https://pytorch.org>). All training and testing were performed on a desktop computer with an Intel Xeon® Gold 6226R CPU, 128 GB RAM, and an NVIDIA RTX 3090 GPU. During the training process, the network weights of the generator and discriminator were initialized using the Xavier method²¹ and optimized using the Adam algorithm,²² with a fixed learning rate of 0.0001, $\beta_1 = 0.5$, $\beta_2 = 0.999$, and batch size of 4. The loss function of the generator and discriminator are described in Methods in Supplemental Material. The total training time for the nonenhanced and contrast-enhanced datasets was \sim 13 h and 10 h, respectively. Once the training process was completed, the parameters of the SynGAN were fixed and adopted for direct transformation of 3T images to corresponding synthetic 7T images. Source code is available from the corresponding author upon reasonable request.

Image Evaluation

The SynGAN was compared with three commonly used medical image synthesis methods, i.e., CycleGAN,²³ U-Net,^{19,24} and WATNet.⁵ The CycleGAN can achieve unsupervised image-to-image translation by using a cycle-consistency loss. The U-Net has the same architecture and details as the generator of the SynGAN. The CycleGAN and U-Net were implemented using the source codes provided in a previous study.¹⁰ The WATNet was implemented using the PyTorch package based on the source codes provided in a previous study.⁵ Two quantitative image quality metrics, peak signal-to-noise ratio (PSNR) and structure similarity (SSIM),²⁵ were used to compared the performance of different synthesis methods on the nonenhanced and contrast-enhanced test data. Both the PSNR and SSIM were only computed over the brain mask.

The qualitative image quality of 3T, 7T, and synthetic 7T images with SynGAN was individually and blindly evaluated by three radiologists (K.C., Y.Q., and C.L. with 6, 8, and 2 years of

TABLE 2. Imaging Parameters for 3T and 7T MRI

Parameter	3T	7T
Slice orientation	Sagittal	Sagittal
Bandwidth (Hz/px)	240	250
Matrix	224 \times 210	320 \times 300
Field of view (mm ²)	224 \times 210	224 \times 210
Slice thickness (mm)	1.0	0.7
Number of slices	176	208–224
Voxel size (mm ³)	1.0 \times 1.0 \times 1.0	0.7 \times 0.7 \times 0.7
Repetition time (msec)	2300	2300
Echo time (msec)	2.99	1.95
Inversion time (msec)	900	1050
Flip angle (degrees)	9	8
Scan time (minute:sec)	4:54	5:14

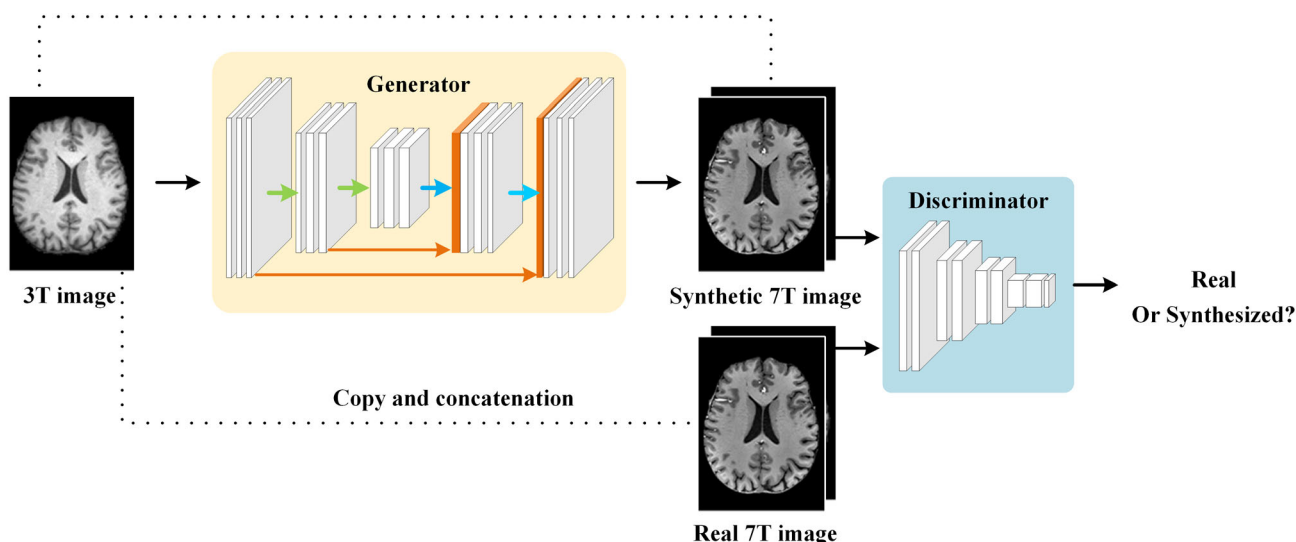


FIGURE 1: The scheme of SynGAN for synthesizing 7T images from 3T images. The SynGAN consists of a generator and a discriminator.

experience in brain MRI interpretation, respectively) in terms of overall image quality, artifacts, sharpness, contrast, and visualization of vessel based on 5-point Likert scales.^{26,27} The evaluations were performed for each subject on a slice-by-slice basis. The criteria for image quality, artifacts, sharpness, contrast, and visualization of vessel assessment on the 5-point Likert scale are presented in Table S1 in the Supplemental Material. The vessel visualization was evaluated based on a previous study of high-quality delineation of intracranial arterial vasculature at 7T MPRAGE MRI.²⁸ Because the deep learning model might introduce “instabilities” in image reconstruction,²⁹ the radiologists also compared the synthetic and real 7T images in a side-by-side manner and evaluated the following: whether the synthetic images removed (yes or no) or introduced (yes or no) important features that may alter the diagnostic interpretation.

Quantitative assessment was based on contrast-to-noise ratio (CNR) by measuring signal intensity in two regions of interest (ROIs).¹⁴ For the nonenhanced test data, the two ROIs were placed in homogeneous regions of white matter and adjacent gray matter. For the contrast-enhanced test data, the two ROIs were placed in homogeneous tumor enhancement region and contralateral normal white matter. Then, the CNR was calculated using the following equation¹³:

$$\text{CNR} = \frac{|\mu_{\text{ROI}_1} - \mu_{\text{ROI}_2}|}{\sqrt{\sigma_{\text{ROI}_1}^2 + \sigma_{\text{ROI}_2}^2}}$$

where μ_{ROI_1} and μ_{ROI_2} are the mean values, and σ_{ROI_1} and σ_{ROI_2} are the standard deviation (SD) of the two ROIs, respectively. The measurement was performed by two radiologists (K.C. and C.L. with 6 and 2 years of experience in brain MRI interpretation, respectively) and calculated per subject. Among the contrast-enhanced test data, two subjects without tumor enhancement were excluded from the CNR assessment.

Statistical Analysis

The image quality scores were compared using Wilcoxon signed rank tests. The CNR values were compared using paired two-tailed

Student's *t* tests. All statistical analyses were performed using SPSS (version 24.0; IBM, Armonk, NY), and statistical significance was set at $P < 0.05$. Interobserver variability was assessed by using intraclass correlation coefficients (ICCs). This coefficient was interpreted as follows: <0.40 , poor agreement; 0.40 – 0.59 , fair agreement; 0.60 – 0.75 , good agreement; and 0.76 – 1.00 , excellent agreement.²⁶

Results

Representative images of 3T, 7T, and synthetic 7T obtained using different synthesis methods are shown in Fig. S2 in the Supplemental Material. The mean PSNR and SSIM values obtained using the different synthesis methods are summarized in Figs. S3 and S4 in the Supplemental Material. The synthetic 7T images with CycleGAN showed obvious artifacts and blurred structures. Although U-Net offered highest PSNR and SSIM values in Figs. S3 and S4 in the Supplemental Material, it resulted in noticeable smooth patterns in the synthetic 7T images. WATNet generates 7T images with improved tissue contrast and certain smooth patterns. SynGAN generated high-quality synthetic images with texture details and perceptual quality comparable to the real 7T images.

Representative 3T, 7T, and synthetic 7T nonenhanced images in a healthy participant and a patient with left middle cerebral artery occlusion are shown in Fig. 2. The synthetic 7T images provide improved sharpness and contrast compared with the 3T images and show comparable image quality to the 7T images. For example, both the real and synthetic 7T images achieve better image contrast among gray matter, white matter and the cerebrospinal fluid. In Fig. 2c, the synthetic 7T images depict the characteristics of the old cerebral infarction that include encephalomalacia and cerebral atrophy. Both the real and synthetic 7T images show intensity inhomogeneities, as indicated by the white arrows in Fig. 2.

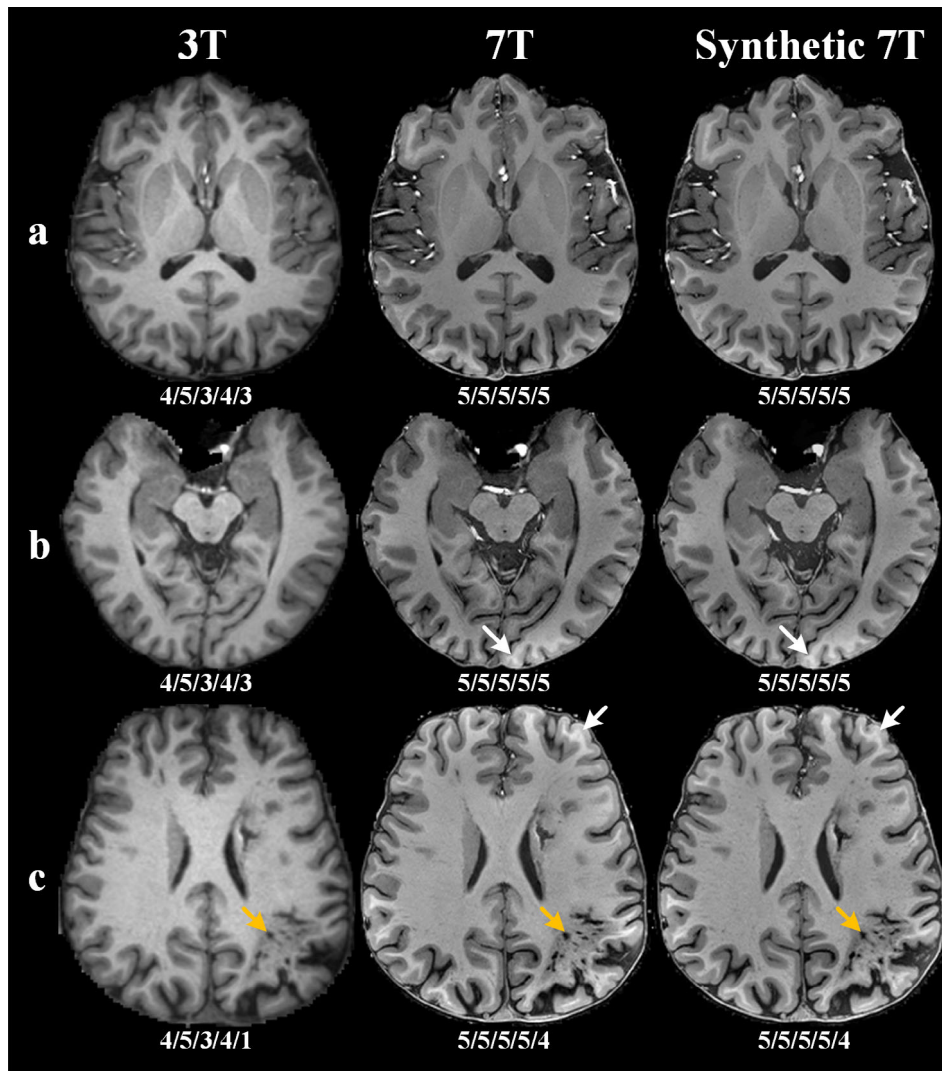


FIGURE 2: Comparisons of representative 3T, 7T, and synthetic 7T nonenhanced images. (a,b) T1-weighted images in a 22-year-old healthy participant. (c) T1-weighted images in a 31-year-old patient with left middle cerebral artery occlusion. Improved tissue contrast and sharpness are observed in the corresponding synthetic 7T images. The golden arrow indicates old cerebral infarction. The white arrows indicate intensity inhomogeneities. The image quality scores (overall image quality/artifacts/sharpness/contrast/visualization of vessel) are listed under each image.

Representative images of 3T, 7T, and synthetic 7T nonenhanced images in the presence of pathologic diseases are shown in Fig. 3. In these patients, the synthetic 7T images show better sharpness and lesion contrast compared with the 3T images, and visually resemble the acquired 7T images for visualization of various pathology, including encephalomalacia (Fig. 3a), demyelination (Fig. 3b), and meningioma (Fig. 3c).

Representative contrast-enhanced T1-weighted images of 3T, 7T, and synthetic 7T are shown in Fig. 4 and Fig. S5 in the Supplemental Material. It can be observed that the synthetic 7T images clearly capture the boundaries, internal architecture, and sharpness of the brain tumors, which are closer to the real 7T images than the 3T images. For example, the synthetic 7T images enable faithful depiction of the ring enhancement and surrounding edema in brain metastases of

lung adenocarcinoma in Fig. 4a, and show the micro-metastases (Fig. S5 in the Supplemental Material) and tiny enhanced lesions in the cystic brain metastases more clearly in Fig. 4b. In Fig. 4c, the synthetic 7T image provides superior depiction of glioma microvasculature compared with the 3T images. In addition, the artifacts in Fig. 4a,c are also successfully removed in the corresponding synthetic 7T images.

Image quality scores for 3T, 7T, and synthetic 7T images are shown in Fig. 5. Compared to nonenhanced T1-weighted images at 3T, the synthetic 7T images achieve significantly higher overall image quality (mean score \pm SD, 5.0 ± 0 for synthetic 7T images and 3.9 ± 0.3 for 3T images), sharpness (mean score, 5.0 ± 0 for synthetic 7T images and 3.1 ± 0.3 for 3T images), contrast (mean score, 5.0 ± 0 for synthetic 7T images and 3.9 ± 0.3 for 3T images), and visualization of vessel (mean score, 3.8 ± 1.0 for

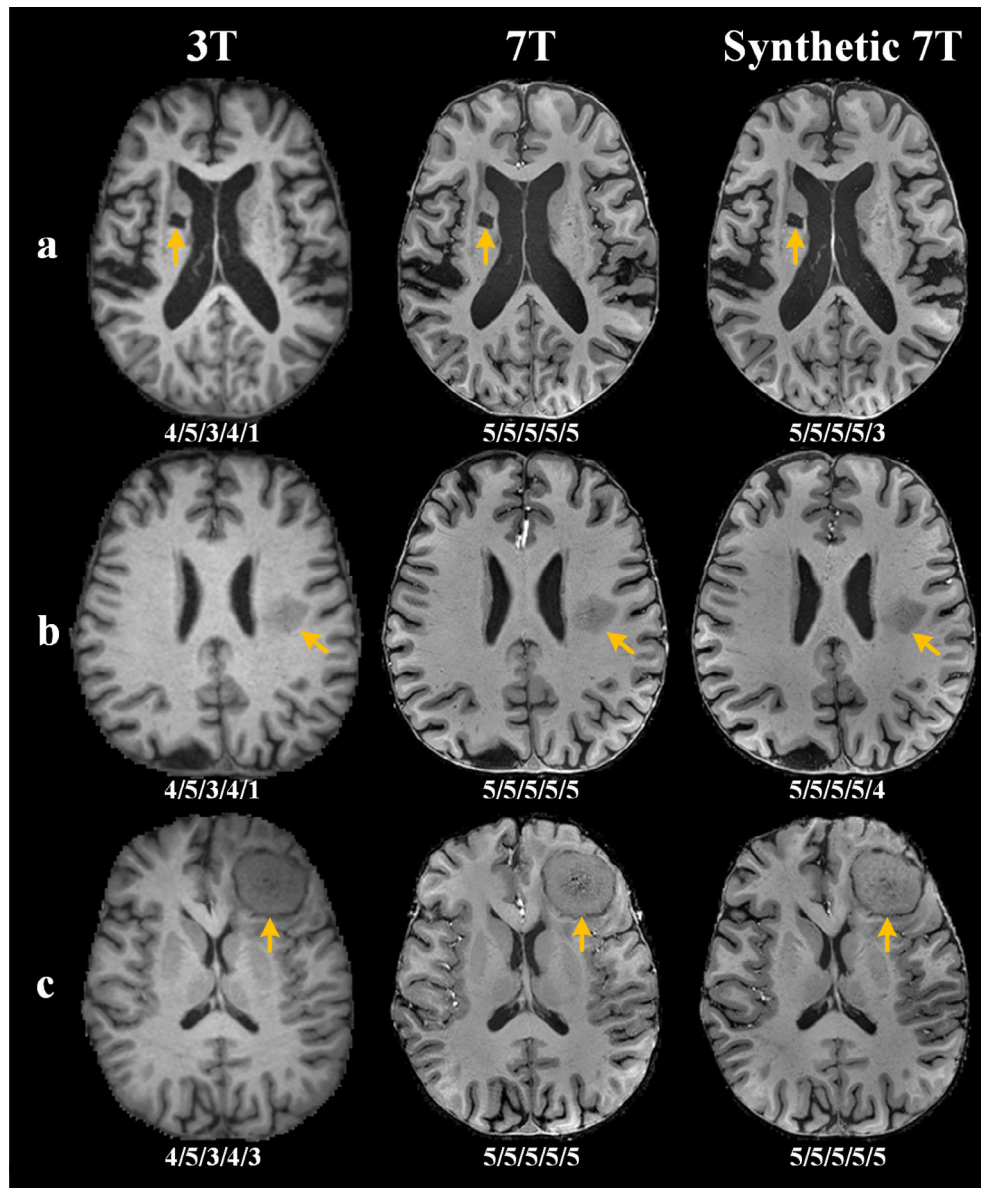


FIGURE 3: Comparisons of representative 3T, 7T, and synthetic 7T nonenhanced images. (a) T1-weighted images in a 70-year-old man with ischemic cerebrovascular disease. (b) T1-weighted images in a 56-year-old man with left paraventricular lesion. (c) T1-weighted images in a 63-year-old woman with meningioma. The synthetic 7T images provide better sharpness and lesion contrast compared with the 3T images. The golden arrows in (a–c) indicate the lesions of encephalomalacia, demyelination, meningioma, respectively. The image quality scores (overall image quality/artifacts/sharpness/contrast/visualization of vessel) are listed under each image.

synthetic 7T images and 1.5 ± 0.9 for 3T images) scores, with no significant difference in artifacts score ($P = 0.317$; mean score, 5.0 ± 0 for synthetic 7T images and 4.8 ± 0.6 for 3T images). Compared to contrast-enhanced T1-weighted images at 3T, the synthetic 7T images achieve significantly higher overall image quality (mean score, 4.9 ± 0.3 for synthetic 7T images and 3.9 ± 0.3 for 3T images), artifacts (mean score, 5.0 ± 0 for synthetic 7T images and 3.9 ± 1.0 for 3T images), sharpness (mean score, 4.7 ± 0.5 for synthetic 7T images and 3.8 ± 0.4 for 3T images), contrast (mean score, 5.0 ± 0 for synthetic 7T images and 3.9 ± 0.3 for 3T images), and visualization of vessel (mean score,

5.0 ± 0 for synthetic 7T images and 4.4 ± 0.5 for 3T images) scores.

For nonenhanced T1-weighted images, there was no significant difference between 7T and synthetic 7T images in terms of all the evaluation criteria, including overall image quality ($P = 0.317$; mean score, 4.9 ± 0.3 for 7T images), artifacts ($P = 0.317$; mean score, 4.9 ± 0.3 for 7T images), sharpness ($P = 1.0$; mean score, 5.0 ± 0 for 7T images), contrast ($P = 1.0$, mean score, 5.0 ± 0 for 7T images), and visualization of vessel ($P = 0.206$, mean score, 4.2 ± 1.3 for 7T images) scores. For contrast-enhanced T1-weighted images, there was also no significant difference

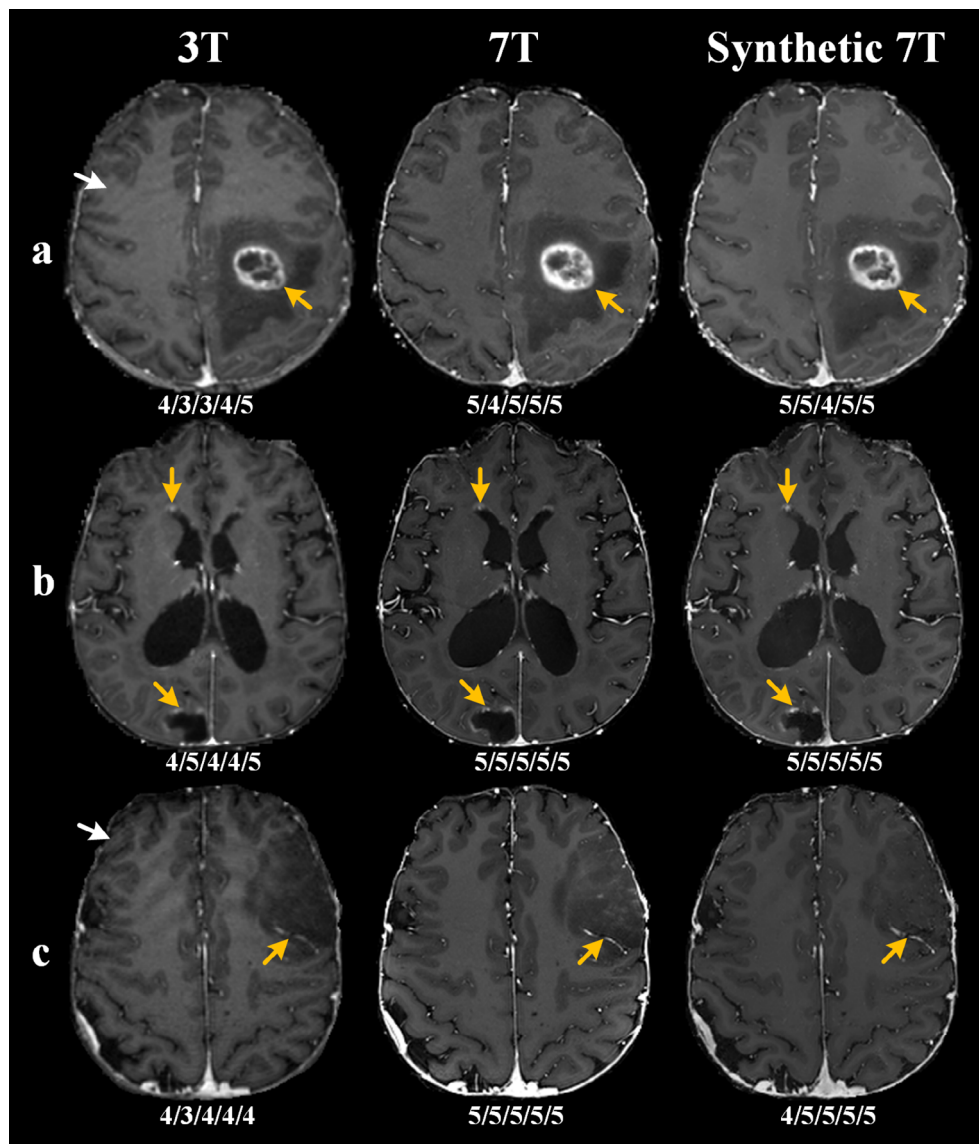


FIGURE 4: Comparisons of representative contrast-enhanced T1-weighted images at 3T, 7T, and synthetic 7T. (a) Images in a 47-year-old man with brain metastases of lung adenocarcinoma. (b) images in a 44-year-old woman with brain metastases of lung adenocarcinoma. (c) Images in a 45-year-old man with low-grade gliomas. The synthetic 7T images can clearly depict the boundaries, internal architecture, and sharpness of the brain tumors. The white arrows indicate motion artifacts. The golden arrows in (a–c) indicate the ring enhancement, tiny enhanced lesion, and feeding artery, respectively. The image quality scores (overall image quality/artifacts/sharpness/contrast/visualization of vessel) are listed under each image.

between 7T and synthetic 7T images in terms of all the evaluation criteria, including overall image quality ($P = 0.317$; mean score, 5.0 ± 0 for 7T images), artifacts ($P = 0.180$; mean score, 4.7 ± 0.7 for 7T images), sharpness ($P = 0.317$; mean score, 4.9 ± 0.3 for 7T images), contrast ($P = 1.0$; mean score, 5.0 ± 0 for 7T images), and visualization of vessel ($P = 1.0$; mean score, 5.0 ± 0 for 7T images) scores.

The CNR assessment results of 3T, 7T, and synthetic 7T images are shown in the boxplots in Fig. S6 in the Supplemental Material. For the nonenhanced test data, the mean CNR values for 3T, 7T, and synthetic 7T images were: 8.19 ± 0.98 , 9.27 ± 1.56 , 9.06 ± 1.46 , respectively. For the contrast-enhanced test data, the mean CNR values for 3T,

7T, and synthetic 7T images were: 6.00 ± 1.53 , 8.80 ± 2.71 , 9.25 ± 2.82 , respectively. For both non-enhanced and contrast-enhanced datasets, the synthetic 7T images offered significantly higher CNR values than the 3T images ($P < 0.05$), with no significant difference compared with the real 7T images ($P = 0.178$ for the nonenhanced test data and $P = 0.214$ for the contrast-enhanced test data).

The interobserver agreement for image quality scores assessment between the three readers were almost excellent for all the evaluation criteria (ICC = 0.791 for overall image quality, ICC = 0.783 for artifacts, ICC = 0.759 for sharpness, ICC = 0.748 for contrast, and ICC = 0.877 for visualization of vessel). The interobserver agreement for CNR

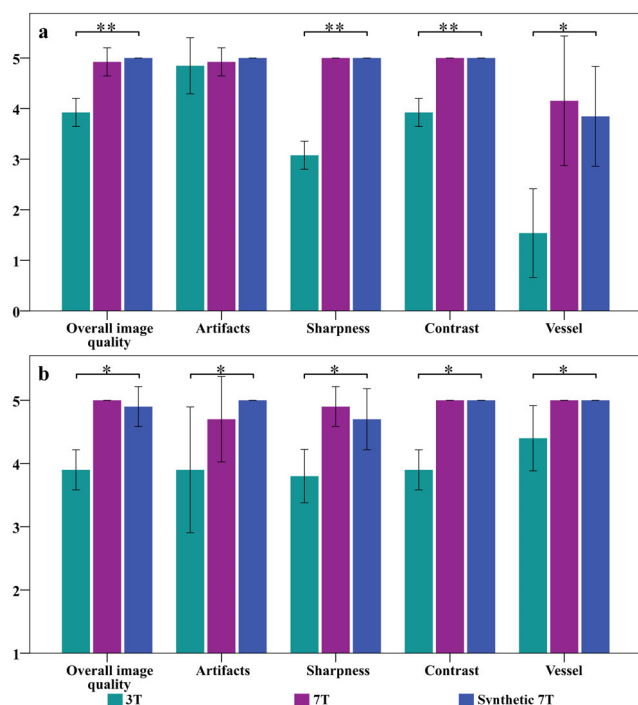


FIGURE 5: Comparisons of qualitative image quality scores between 3T, 7T, and synthetic 7T images for nonenhanced (a) and contrast-enhanced (b) T1-weighted images. Image quality scores were evaluated independently by three blinded readers in terms of overall image quality, artifacts, sharpness, contrast, and visualization of vessel. Error bars are SD across the test data. *Statistically different results with $P < 0.05$, ** denotes $P < 0.001$.

assessment between the two readers were also excellent in both the nonenhanced (ICC = 0.900) and contrast-enhanced (ICC = 0.944) datasets. Moreover, the synthetic images did not remove or introduce important features in either the non-enhanced or contrast-enhanced test data. Average synthetic time was 11.4 msec per slice (2.95 sec per participant) for SynGAN in PyTorch on the RTX 3090 GPU.

Discussion

In this study, we developed and clinically evaluated a SynGAN approach for synthesizing high quality 7T images from 3T images. Our results show that the synthetic 7T images significantly outperform the 3T images in terms of overall image quality, sharpness, contrast, and visualization of vessel for both nonenhanced and contrast-enhanced test data. In addition, SynGAN can provide comparable performance to acquired 7T images in terms of overall image quality, artifact, sharpness, and contrast. The SynGAN approach enables synthetic speeds of ~ 11 msec per slice, which allows real-time generation of synthetic 7T images for practical clinical deployment.

In recent years, there has been marked progress in deep learning methods to resolve various medical image synthesis

tasks, focusing on multimodal MR image synthesis^{8,10} or cross-modality image synthesis (eg, MRI-to-CT synthesis).³⁰ Synthesis of 7T images from the corresponding 3T images is challenging because the two images differ not only in resolution, but also in contrast.⁵ In this work, we adopted a GAN-based framework to learn the complex 3T-to-7T mapping, because GAN can effectively capture the high frequency details in the target image and have achieved promising results in synthesizing various types of medical image.⁹ Our results show that SynGAN is capable of synthesizing 7T images with improved tissue contrast and sharpness that are similar to the acquired 7T images. The improved tissue contrast is promising as it may assist in more accurate brain tissues or substructures (eg, hippocampal subfields) segmentation, which is a fundamental step in functional MRI analysis.

In our study, CycleGAN showed inferior performance in synthesizing 7T images, which may be attributed to the fact that cycle-consistency is sensitive to perturbation and may produce multiple plausible solutions.¹⁰ In terms of PSNR and SSIM, U-Net with pixel-wise loss alone achieved the best performance. Nevertheless, minimizing pixel-wise loss encourages finding pixel-wise averages of plausible solutions which are typically overly-smooth and have poor perceptual quality.³¹ Therefore, GAN based model is not designed and trained to achieve the highest PSNR as this does not capture the visual perception and texture details.³²

Although previous studies have demonstrated the feasibility of synthesizing 7T image using deep learning, the applicability of this method for clinical brain imaging is yet to be explored.⁴⁻⁶ Therefore, test data with different clinical indications were used to evaluate the performance of synthetic 7T images in this study. Example results show that the synthetic 7T images may provide clear visualization of a wide range of pathology, including encephalomalacia, demyelination, and brain tumor. Furthermore, the contrast-enhanced T1-weighted images at synthetic 7T may enhance visualization of tumor boundaries, internal architectures, as well as subtle pathology. This may be particularly beneficial in refining radiation target volume delineation or improving completeness of tumor resection.³³ In addition, the synthetic 7T images enabled better depiction of microvascular properties of gliomas, which is useful for predicting tumor grade and better characterize microscopic infiltration.²

Patient abnormalities are heterogeneous, and some abnormalities are rare and unlikely to be included in the training data set.³⁴ In addition, image synthesis is an ill-posed problem and has intrinsic uncertainty.³⁵ Therefore, one of the most important concerns of image synthesis with deep learning is whether they can faithfully generate abnormalities in clinical practice. Although spurious features or removal of abnormalities are not observed in the synthetic 7T images in our study, it is important to quantify and

display the pixel-wise synthetic uncertainty for clinical translation and deployment.³⁶

Limitations

First, the T1-weighted images at 7T were acquired using the MPRAGE sequence, which suffers from strong intensity inhomogeneities due to B1 field inhomogeneities.¹³ This results in poor visualization of subtentorial structures (eg, cerebellum) and may be alleviated by using the MP2RAGE sequence in future study.³⁷ Second, considering the safety concerns about Gadolinium-based contrast agents in the medical community,³⁸ we acquired the contrast-enhanced 3T and 7T MRI data with a single injection of contrast agent, which raises a question about the potential influence of the time interval between the two MRI measurements. Although our paired 3T and 7T acquisitions were performed within the time range before the enhanced signal decrease,³⁹ it would be more appropriate to acquire contrast-enhanced 7T MRI immediately after contrast agent administration in future studies. Third, synthetic 7T image generation was evaluated on a small number test data with heterogeneous pathology and MRI scans from a single scanner with minimal variations in imaging parameters. In the future, additional evaluation on prospective datasets with variable clinical settings and MRI scanners will be performed to further demonstrate the clinical potential of the synthetic 7T images.

Conclusion

The synthetic 7T images with generative adversarial network achieved high image quality and good tissue contrast, potentially providing an alternative way to achieve the advantages of ultra-high field 7T MRI in clinical brain imaging.

REFERENCES

1. Tractnig S, Springer E, Bogner W, et al. Key clinical benefits of neuroimaging at 7 T. *Neuroimage* 2018;168:477-489.
2. Rutland JW, Delman BN, Gill CM, Zhu C, Shrivastava RK, Balchandani P. Emerging use of ultra-high-field 7T MRI in the study of intracranial vascularity: State of the field and future directions. *AJNR Am J Neuroradiol* 2020;41:2-9.
3. Balchandani P, Naidich TP. Ultra-high-field MR neuroimaging. *AJNR Am J Neuroradiol* 2015;36:1204-1215.
4. Bahrami K, Shi F, Reikik I, Gao Y, Shen D. 7T-guided super-resolution of 3T MRI. *Med Phys* 2017;44:1661-1677.
5. Qu L, Zhang Y, Wang S, Yap PT, Shen D. Synthesized 7T MRI from 3T MRI via deep learning in spatial and wavelet domains. *Med Image Anal* 2020;62:101663.
6. Zhang Y, Cheng JZ, Xiang L, Yap PT, Shen D. Dual-domain cascaded regression for synthesizing 7T from 3T MRI. In: Frangi AF, Schnabel JA, Davatzikos C, Alberola-López C, Fichtinger G, editors. *International conference on medical image computing and computer-assisted intervention*. Cham, Switzerland: Springer; 2018. p 410-417.
7. You SH, Cho Y, Kim B, Yang KS, Kim BK, Park SE. Synthetic time of flight magnetic resonance angiography generation model based on cycle-consistent generative adversarial network using PETRA-MRA in the patients with treated intracranial aneurysm. *J Magn Reson Imaging* 2022;56:1513-1528.
8. Benzakoun J, Deslys MA, Legrand L, et al. Synthetic FLAIR as a substitute for FLAIR sequence in acute ischemic stroke. *Radiology* 2022;303:153-159.
9. Nie D, Trullo R, Lian J, et al. Medical image synthesis with deep convolutional adversarial networks. *IEEE Trans Biomed Eng* 2018;65:2720-2730.
10. Kong L, Lian C, Huang D, et al. Breaking the dilemma of medical image-to-image translation. *Adv Neural Inf Process Syst* 2021;34:1964-1978.
11. Qu L, Wang S, Yap PT, Shen D. Wavelet-based semi-supervised adversarial learning for synthesizing realistic 7T from 3T MRI. In: Shen D, Liu T, Peters TM, Staib LH, Essert C, Zhou S, Yap PT, Khan A, editors. *International conference on medical image computing and computer-assisted intervention*. Cham, Switzerland: Springer; 2019. p 786-794.
12. Wei J, Pan Y, Xia Y, Shen D. Learning to synthesize 7 T MRI from 3 T MRI with few data by deformable augmentation. In: Lian C, Cao X, Reikik I, Xu X, Yan P, editors. *Machine learning in medical imaging*. Cham, Switzerland: Springer; 2021. p 70-79.
13. Oliveira IAF, Roos T, Dumoulin SO, Siero JCW, Van der Zwaag W. Can 7T MPRAGE match MP2RAGE for gray-white matter contrast? *Neuroimage* 2021;240:118384.
14. Cheng K, Duan Q, Hu J, et al. Evaluation of postcontrast images of intracranial tumors at 7T and 3T MRI: An intra-individual comparison study. *CNS Neurosci Ther* 2023;29:559-565.
15. Tustison NJ, Avants BB, Cook PA, et al. N4ITK: Improved N3 bias correction. *IEEE Trans Med Imaging* 2010;29:1310-1320.
16. Iglesias JE, Liu CY, Thompson PM, et al. Robust brain extraction across datasets and comparison with publicly available methods. *IEEE Trans Med Imaging* 2011;30:1617-1634.
17. Jenkinson M, Bannister P, Brady M, Smith S. Improved optimization for the robust and accurate linear registration and motion correction of brain images. *Neuroimage* 2002;17:825-841.
18. Isola P, Zhu JY, Zhou T, et al. Image-to-image translation with conditional adversarial networks. *Proceedings of the IEEE Conference on Computer Vision and Pattern Recognition*. Piscataway, NJ: IEEE; 2017. p 1125-1134.
19. Jin KH, McCann MT, Froustey E, Unser M. Deep convolutional neural network for inverse problems in imaging. *IEEE Trans Image Process* 2017;26:4509-4522.
20. Duan C, Deng H, Xiao S, et al. Fast and accurate reconstruction of human lung gas MRI with deep learning. *Magn Reson Med* 2019;82:2273-2285.
21. Glorot X, Bengio Y. Understanding the difficulty of training deep feedforward neural networks. *Proceedings of the 13th International Conference on Artificial Intelligence and Statistics*. Sardinia, Italy: PMLR; 2010. p 249-256.
22. Kingma DP, Ba J. Adam: A method for stochastic optimization. *arXiv Preprint arXiv:1412.6980* 2014.
23. Zhu JY, Park T, Isola P, et al. Unpaired image-to-image translation using cycle-consistent adversarial networks. *Proceedings of the IEEE International Conference on Computer Vision*. Piscataway, NJ: IEEE; 2017. p 2223-2232.
24. Ronneberger O, Fischer P, Brox T. U-net: Convolutional networks for biomedical image segmentation. In: Navab N, Hornegger J, Wells WM, Frangi AF, editors. *International conference on medical image computing and computer-assisted intervention*. Cham, Switzerland: Springer; 2015. p 234-241.
25. Wang Z, Bovik AC, Sheikh HR, Simoncelli EP. Image quality assessment: From error visibility to structural similarity. *IEEE Trans Image Process* 2004;13:600-612.
26. Chen F, Taviani V, Malkiel I, et al. Variable-density single-shot fast spin-echo MRI with deep learning reconstruction by using variational networks. *Radiology* 2018;289:366-373.

27. Kim M, Kim HS, Kim HJ, et al. Thin-slice pituitary MRI with deep learning-based reconstruction: Diagnostic performance in a postoperative setting. *Radiology* 2021;298:114-122.
28. Umutlu L, Theysohn N, Maderwald S, et al. 7 tesla MPRAGE imaging of the intracranial arterial vasculature: Nonenhanced versus contrast-enhanced. *Acad Radiol* 2013;20:628-634.
29. Antun V, Renna F, Poon C, Adcock B, Hansen AC. On instabilities of deep learning in image reconstruction and the potential costs of AI. *Proc Natl Acad Sci U S A* 2020;117:30088-30095.
30. Jans L, Chen M, Elewaut D, et al. MRI-based synthetic CT in the detection of structural lesions in patients with suspected sacroiliitis: Comparison with MRI. *Radiology* 2021;298:343-349.
31. Ledig C, Theis L, Huszár F, et al. *Photo-realistic single image super-resolution using a generative adversarial network. Proceedings of the IEEE conference on computer vision and pattern recognition.* Piscataway, NJ: IEEE; 2017. p 4681-4690.
32. Mardani M, Gong E, Cheng JY, et al. Deep generative adversarial neural networks for compressive sensing MRI. *IEEE Trans Med Imaging* 2018;38:167-179.
33. Regnery S, Knowles BR, Paech D, et al. High-resolution FLAIR MRI at 7 tesla for treatment planning in glioblastoma patients. *Radiother Oncol* 2019;130:180-184.
34. Duan C, Xiong Y, Cheng K, et al. Accelerating susceptibility-weighted imaging with deep learning by complex-valued convolutional neural network (ComplexNet): Validation in clinical brain imaging. *Eur Radiol* 2022;32:5679-5687.
35. Tanno R, Worrall DE, Kaden E, et al. Uncertainty modelling in deep learning for safer neuroimage enhancement: Demonstration in diffusion MRI. *Neuroimage* 2021;225:117366.
36. Edupuganti V, Mardani M, Vasanawala S, Pauly J. Uncertainty quantification in deep MRI reconstruction. *IEEE Trans Med Imaging* 2020;40:239-250.
37. O'Brien KR, Magill AW, Delacoste J, et al. Dielectric pads and low-adiabatic pulses: Complementary techniques to optimize structural T1w whole-brain MP2RAGE scans at 7 tesla. *J Magn Reson Imaging* 2014;40:804-812.
38. Gulani V, Calamante F, Shellock FG, Kanal E, Reeder SB, International Society for Magnetic Resonance in Medicine. Gadolinium deposition in the brain: Summary of evidence and recommendations. *Lancet Neurol* 2017;16:564-570.
39. Noebauer-Huhmann IM, Szomolanyi P, Kronnerwetter C, et al. Brain tumours at 7T MRI compared to 3T—Contrast effect after half and full standard contrast agent dose: Initial results. *Eur Radiol* 2015;25:106-112.